
DETECTION OF DOUBLE NUCLEI GALAXIES IN SDSS

Anwesh Bhattacharya

Department of Physics

Department of CSIS

Birla Institute of Technology and Science
Pilani, Rajasthan, India

f2016590@pilani.bits-pilani.ac.in

Snehanshu Saha

Department of CSIS

APPCAIR

Birla Institute of Technology and Science
Goa, India

snehanshus@goa.bits-pilani.ac.in

Mousumi Das

Indian Institute of Astrophysics

Bangalore, India

mousumi@iiap.res.in

ABSTRACT

It is now well established that galaxy interactions and mergers play a crucial role in the hierarchical growth of structure in our universe. Galaxy mergers can lead to the formation of elliptical galaxies and larger disk galaxies, as well as drive galaxy evolution through star formation and nuclear activity. During mergers the nuclei of the individual galaxies come closer and finally form a double nuclei galaxy. Although mergers are common, the detection of double-nuclei galaxies (DNGs) is rare and fairly serendipitous. Their detection is very important as their properties can help us understand the formation of supermassive black hole (SMBH) binaries, dual active galactic nuclei (DAGN) and the associated feedback effects. There is thus a need for an automatic/systematic survey of data for the discovery of double nuclei galaxies. Using the Sloan digital sky survey (SDSS) as the target catalog, we have introduced a novel algorithm GOTHIC — *Graph-Boosted iterated Hill Climbing*[13] — that detects whether a given image of a galaxy has characteristic features of a DNG (ASCL entry 2707). We have tested the algorithm on a random sample of 100,000 galaxies from the Stripe 82[2] region in SDSS and obtained a maximum detection rate of 4.2% with a careful choice of the input catalog.

1 Introduction

A galaxy is a system of stars, interstellar gas, dust and dark matter bounded by gravitational forces. Based on their morphology galaxies are categorized as spiral, irregular or elliptical. Galaxies are not usually isolated systems but are instead clustered into galaxy groups and large galaxy clusters [18]. Hence, galaxies often interact tidally at a distance with each other or undergo mergers with one another. During these interactions the gravitational field of one galaxy affects the other one. If the two galaxies do not have enough momentum to continue to travel after interacting, they will finally collide and merge, leading to the formation of a galaxy merger remnant [5]. Galaxy mergers are common in our universe and are one of the main drivers of galaxy evolution [7, 1].

The outcome of galaxy mergers depends on the mass ratio of the merging galaxies. In the cases where one galaxy is much more massive than the other one, the more massive galaxy remains more or less intact whereas the smaller galaxy is tidally stripped of a large fraction of its mass and finally becomes part of the larger galaxy. Such mergers are called galaxy accretion events or minor mergers. When the colliding galaxies are similar in mass and size, it is called a major merger event. Major mergers usually lead to the formation of elliptical galaxies. Another classification system for galaxy mergers depends on the presence of cold interstellar gas. When one or both the galaxies are gas rich, the merger is said to be a wet merger and when both galaxies are gas free, as in ellipticals, the merger is said to be a dry merger. However, wet or dry, major or minor, all mergers can lead to the formation of a single envelope containing two nuclei. Such dual nuclei systems represent the final stage of galaxy mergers [15].

As the galaxies merge, the supermassive black holes (SMBHs) in their nuclei come closer and may start accreting mass. Such accreting SMBHs are called active galactic nuclei (AGN) and give out large amounts of energy over the whole electromagnetic spectrum and can be detected using optical, radio or X-ray telescopes [31]. Alternatively, the large gas infall into the nuclear regions can trigger starburst activity. Thus double nuclei galaxies can host AGN pairs, AGN-starburst pairs or starburst nuclei in their centers [33]. When two AGN are found in a merger remnant, they can form a dual AGN (DAGN) if the nuclei are separated by <10 Kpc. AGN pairs at separations of a few parsecs or $<<1$ Kpc are called binary AGN (BAGN). The number of DAGN identified till now is less than 50 [32] and the number of binary AGN identified is less than 5 [23].

There are several reasons why we need to find more DAGN or BAGN. The first reason is that they represent SMBHs coming closer together in galaxies. At distances of several Mpc and beyond the local universe, the only way to detect SMBHs is through the radiation emitted from AGN activity. The mass of the SMBH pairs affects the stellar and gas content of the nuclear regions of the galaxies, triggering disk instabilities and star formation. Secondly, although DAGN are rare in the universe, their study is important for understanding the growth of SMBHs as it is suggested that merger-triggered AGN may dominate SMBH growth [22]. Third, SMBH binaries represent black holes that will eventually merge and produce gravitational radiation [21]. Although the gravitational radiation will be emitted only when the SMBHs are at very close separations, a larger sample of DAGN will help us understand the evolutionary path for such systems. Fourth, AGN give out enormous amounts of radiation that can push gas out from the nuclear region and even beyond the galaxy. This is called AGN feedback and it can result in the growth the circumgalactic medium around galaxies [16]. The gas can also fall back onto the disks resulting in star formation. In the past decade it has become clear that AGN feedback is important for galaxy evolution, and if there is an AGN pair then the effect will be even more important not only because of two AGN in the galaxy center, but also because the AGN winds can overlap and produce additional feedback effects. Hence, large samples of DAGN are essential for fully understanding the role of mergers in galaxy evolution.

The earlier DAGNs have been *serendipitously* discovered [9, 24, 35, 37], mainly during galaxy surveys of emission line galaxies and merger remnants. Later studies used samples of double peaked AGN emission line galaxies (DPAGN) to search for DAGN [44]. However, DPAGN can also be due to AGN outflows or rotating disks. So one of the best ways in which to detect DAGN is by identifying individual nuclei in a dual nuclei galaxy [34]. The existing surveys of galaxy pairs are either too small [20] or the galaxy separations are too large to include merger remnants [30]. Thus a deeper and larger catalog is necessary in order to do statistical studies of dual nuclei galaxies and identify DAGN. The detection of previously undiscovered samples is essential for understanding the final stages of the galaxy merging process. Hence, there is a need of a pipeline to sift through a large catalog of galaxies and steadily increase the pool of candidate DAGNs. The aim of this paper is to develop an algorithm that extracts images from the Sloan Digital Sky Survey (SDSS) survey and identifies a pool of dual nuclei systems that we will use later for identifying a large sample of DAGN.

2 Previous Studies, Test Sample and Input Catalog

As mentioned in the previous section, galaxies with two nuclei separated by kiloparsec scales are known as DAGN, whereas, the ones in which the separation is of the order of parsecs are called binary AGN. The hierarchical model of structure formation predicts the formation of such gravitationally bound binary SMBHs. The accretion of mass onto the nuclei transforms the nuclei into AGN and is an important part of SMBH growth and galaxy evolution. Moreover, these galaxy merger events could ultimately give rise to black-hole merger events which are crucial for gravitational wave detection [3]. There have been several studies of double nuclei galaxies at different wavelengths. In this section we discuss these previous studies and describe the test sample which we finally use for testing our algorithm.

The main catalog that we used for testing the algorithm developed in this paper is from *Gimeno* et. al. [20]. The relevance of galaxy interactions and minor mergers in the formation of double-nuclei galaxies, the correlation between geometric and photometric parameters of the nuclei and their host galaxies, have been investigated in this study. It also discusses the differences or similarities between the component nuclei and their location in the host system. The galaxies selected had systematic velocities cz , and redshifts z in the range $cz < 15000$ km/s, $z < 0.05$, $m_B < 18$. *Mezcua* et. al. [28] did further studies of this sample using observations. In their study, the luminosity of the nuclei and their relative separations were derived from the multi-component photometric fits to the galaxies in the r-band *SDSS* optical images. A majority of the sources have projected separations ≤ 4 kpc. The ratio of nuclear luminosities indicated that most of the systems were in the final stages merging. This was supported by the existence of a single galaxy disk in 65% of the systems studied and the significant correlation between nuclear luminosity and host luminosity for the

single-disk systems. The sources fitted with a single disk are in a more evolved stage of the merging process and present an enhancement of the nuclear luminosity compared to the double-disk systems.

Koss et. al. [26] have mentioned the difficulty of resolving each AGN in optical and X-ray observations. The *Swift Burst Alert Telescope* survey was used to create a catalog of 167 AGN out of which 81 have a close companion within a 100 kpc radius. *MRK 739* (also listed as *NGC 3758* in *Gimeno et. al* [20]) has been well known since 1986 due to the paper by *Netzer et. al* [29]. In another work by *Koss et. al* [27], SDSS optical imaging and observations from the *Chandra X-ray Observatory* were utilized to rule out the possibility of *MRK 739W* (the nuclei on the western side) being a starburst region, which was suggested by its optical spectra. *MRK 739E* was already known to be an AGN due to *Netzer* [29]. It is interesting to note that the optical spectra of *MRK 739E* and *MRK 739W* both have a peak around 6750 Angstrom that falls under the R-band of the SDSS filters.

The detection of double-nuclei galaxies is important from the point of view of Cosmology and Structure Formation. *Davis* [17] and *Springel* [39] have suggested that galaxy interactions play an important role in the growth of their central SMBH. It has been suggested theoretically that DAGN must be found in relative abundance in our universe [25]. However, such objects are rarely found as most of them are radio-quiet and are difficult to resolve in the optical. Previously, double-peaked narrow emission lines were used as the criteria for a galaxy to be a candidate DAGN. However, such a criteria has received criticism as similar observations can be drawn from other phenomenon in single active nuclei galaxies itself (*Xu & Komossa* [42]). This suggests that alternative methods must be devised to procure candidates for DAGN galaxies. For example radio observations have used the *Very Large Baseline Array* (VLBA) to identify DAGN candidates [19]. There have been efforts towards studying individual DAGNs such as *MRK 739* by *Koss et al.* [27], *MRK 463* by *Bianchi* [6] and *ARP 299* by *Ballo et al.* [4]. *Rubinur et al.* [33] have conducted radio-studies on a sample of DPAGN. Hence, it is an important task to increase the pool of DAGN candidates for robust statistical studies. In this paper, we have focused on detecting the presence of dual nuclei given a $40'' \times 40''$ r-band image of a galaxy from the SDSS images of galaxies. This sample will form the basic sample for a followup study aimed at deriving a large sample DAGN in SDSS.

2.1 Selected Samples from Pre-Existing Catalogs

Mezcua et. al. [28] have reported that out of the 107 galaxies in the *Gimeno* catalog, only 60 have imaging data in SDSS DR8. Two galaxies, *NGC-3758* and *MRK-212* are shown as representatives in figure (1). The former has gained some attention outside the astronomy community due to its symmetric morphology [40, 43], and the latter has been extensively studied in multiple wavelengths [32]. The algorithm is domain-specific and hence a pre-existing sample was necessary for its development and testing. We have chosen the *Gimeno* catalog [20] as our test sample, and *GOTHIC* has achieved 100% accuracy on this dataset. The images have been selected from SDSS.

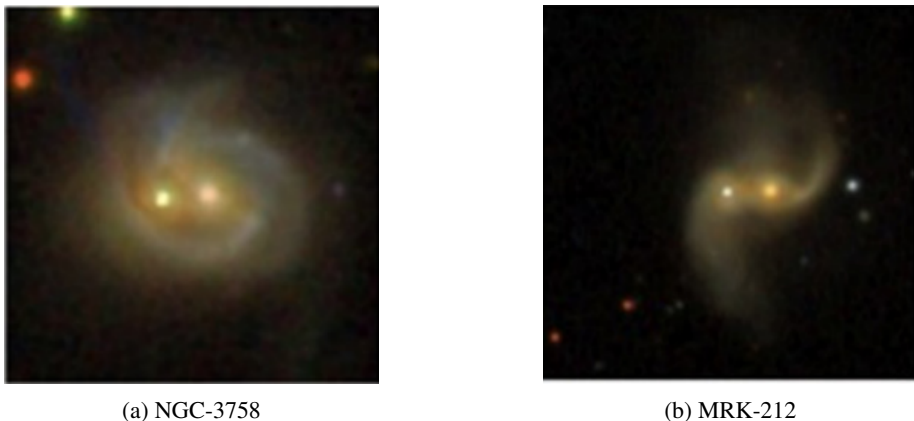


Figure 1: Double-Nuclei Galaxies Sample

2.2 Input Catalog

Our input dataset is located in this public [folder](#). It contains the entire SDSS and Gaia catalog in the Stripe-82 region, which was used for crossmatching (section 5.2), in the files *SDSS_Strip82_All.csv* and *Gaia_Strip82_All.csv*, respectively.

3 The GOTHIC Algorithm

The FITS data of the given source, in all the SDSS bands (ugriz) were downloaded and subsequently a cutout of $40''$ centred around the source was performed. The algorithm works individually for each band. The sequence of steps can be described as follows -

1. Scaling/Smoothing of the image for ease of visualisation
2. Edge detection with Canny to approximate galaxy envelope
3. Sersic profile fitting to infer noise/signal levels
4. Peak detection by Iterated Hill Climbing
5. Identification of the galaxy as single/double-nuclei or neither, based on graph searching

Given below is the formal pseudocode for the algorithm, the details of which have been explained in Appendix A. The result of running GOTHIC is shown in figure (2)

GOTHIC(*cood, frame*)

```

1   $\triangleright$  cood - Celestial coordinates of an object
2   $\triangleright$  frame - FITS frame containing the object
3  img  $\leftarrow$  CUTOOUT (frame, cood, 40'')                                 $\triangleright$  Returns a  $40''$  cutout image
4  img  $\leftarrow$  LOG-NORMALIZE (img)                                      $\triangleright$  Step 1
5  img  $\leftarrow$  GAUSSIAN-KERNEL (img, 5, 5)                                 $\triangleright$  Step 1
6  edges  $\leftarrow$  CANNY (img)                                          $\triangleright$  Step 2
7  hull, reg  $\leftarrow$  CONVEX-HULL (edges)                                 $\triangleright$  Step 2
8  noise, signal  $\leftarrow$  SERSIC-FIT (img, reg)                                 $\triangleright$  Step 3
9  sreg  $\leftarrow$  SEARCH-REGION (img, reg, noise)                                 $\triangleright$  Step 4
10 peak_list  $\leftarrow$  ITERATED-HILL-CLIMB (sreg, img, 500)                 $\triangleright$  Step 4
11 verdict  $\leftarrow$  CLASSIFY (peak_list, sreg, img, signal)                 $\triangleright$  Step 5
12 return verdict

```

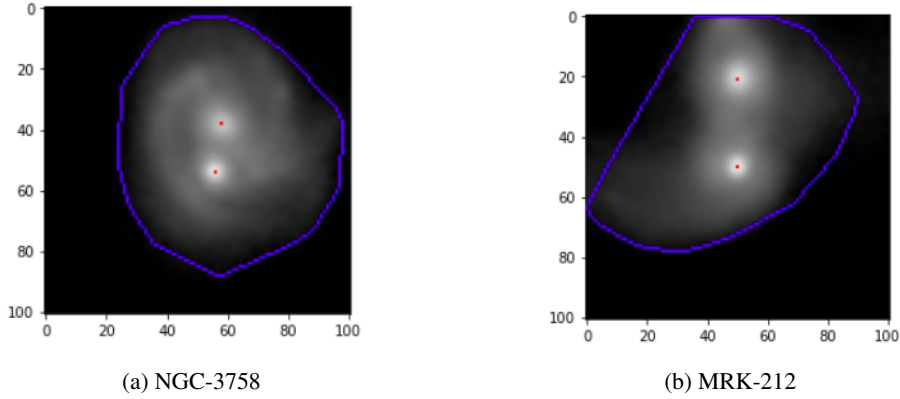


Figure 2: Detected peaks from GOTHIC

4 Mathematical Basis for Classification and Related Procedures

In this section, we detail lines 10 and 11 of GOTHIC. The procedure `SEARCH-REGION` extracts the region inside the blue border, as shown in figure (2). Drawing of the border, in which the galaxy of interest lies in the cutout image, is required by the classification procedure. Moreover, it is also dependent on the Sersic [36] light-profile parameters of the galaxy. Parameter fitting has been performed explicitly using `scipy`, instead of depending on derived parameters of the SDSS catalog. These steps have been detailed in Appendix A.

4.1 Iterated Hill Climbing

To identify the intensity peaks in the image, it is tempting to sort the pixels in descending order of pixel value and extract the top few pixels. This, however, does not give sufficient information to classify the object as a single-nuclei or double-nuclei galaxy. The top two pixels extracted are likely to be pixel neighbors near the brightest peak. Due to the high chance of foreground stars, which are brighter than the central galaxy, appearing in the field of view, it might lead to erroneous detections. The robust definition of a peak is a pixel whose value is greater than all of its neighbors. Finding a peak is achieved by a discrete hill-climbing algorithm, operating on a 2-D image. We have allowed for an angular resolution of $1''$, which translates to a separation of 3 pixels in the cutout image. Hence, the neighbor of a pixel is defined to be the 7×7 square grid centred on it.

```

HILL-CLIMB(pt, reg, img)
1   $\triangleright$   $pt$  - starting point
2   $\triangleright$   $reg$  - search region
3   $\triangleright$   $img$  - underlying image
4   $newpt \leftarrow \text{NULL}$ 
5  while  $pt \neq newpt$ 
6    do  $neighs \leftarrow \text{NEIGHS-IN-REG}(pt, reg)$        $\triangleright$  Returns the  $7 \times 7$  grid neighbors centred at  $pt$ 
7     $newpt \leftarrow pt$ 
8    for  $n$  in  $neighs$ 
9      do if  $img[n] > img[newpt]$ 
10        then  $newpt \leftarrow n$ 
11     $pt \leftarrow newpt$ 
12  return  $newpt$ 

```

The input point pt is initialised randomly within the search region reg . The procedure is guaranteed to terminate as the pixel value of pt strictly increases in each iteration until no greater neighbor, centred about it, can be found. ITERATED-HILL-CLIMB iterates over HILL-CLIMB, by seeding random initial points in the search region, and returns a list of peaks thus obtained. It is also to be noted that a peak is accepted only if its signal to noise ratio > 3 . Figure (3) shows the output for example double-nuclei galaxies.

```

ITERATED-HILL-CLIMB(reg, img, iter)
1   $\triangleright$   $reg$  - search region
2   $\triangleright$   $img$  - underlying image
3   $\triangleright$   $iter$  - number of iterations to perform
4   $peak\_list \leftarrow []$                                  $\triangleright$  Empty list
5   $i \leftarrow 0$ 
6  repeat  $pt \leftarrow \text{CHOOSE-RANDOM}(reg)$            $\triangleright$  Returns a random point in the region  $reg$ 
7     $peak \leftarrow \text{HILL-CLIMB}(pt, reg, img)$ 
8    if  $peak$  not in  $peak\_list$  and  $\text{SNR}(peak) \geq 3$ 
9      then  $\text{APPEND}(peak, peak\_list)$                    $\triangleright$  Adds  $peak$  to the list  $peak\_list$ 
10    $i \leftarrow i + 1$ 
11 until  $i = iter$ 
12 return  $peak\_list$ 

```

4.2 Graph-Searching and Classification

The peaks in $peak_list$ comprise local maxima, the global maxima, and the peak(s) corresponding to the central object in the image. It is the latter which is ascertained by graph-searching. This is exhibited by the sample cases in figure (3a), where ITERATED-HILL-CLIMBING detects a peak on an offset stray object, and figure (3b), where multiple peaks are detected in the object of interest. The procedure CLASSIFY processes the list of peaks and returns one of the three verdicts - NO_PEAK, SINGLE or DOUBLE

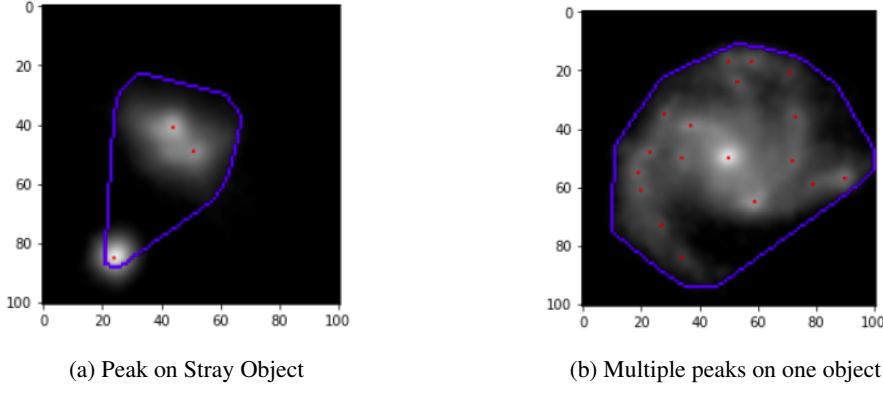


Figure 3: Optima from ITERATED-HILL-CLIMBING

CLASSIFY(*peak_list*, *reg*, *img*, *signal*)

```

1   $\triangleright$  reg - search region
2   $\triangleright$  peak_list - peak list
3   $\triangleright$  img - underlying image
4  comps  $\leftarrow$  CONNECTED-COMPONENTS (reg)            $\triangleright$  Runs depth-first-search
5  SORT-BY-DISTANCE (comps)
6  group  $\leftarrow$  FIRST-GROUP (comps)
7  lcmp  $\leftarrow$  LARGEST-COMPONENT (group)
8  pks  $\leftarrow$  FIND-PEAKS-IN (lcmp, peak_list)
9  pks  $\leftarrow$  FILTER-BY-INTENSITY (pks, img, signal)
10 len  $\leftarrow$  LENGTH (pks)
11 if len  $\geq 2$ 
12   then return DOUBLE
13 elseif len = 1
14   then return SINGLE
15 else return NO_PEAK

```

The cutout image is treated as a graph $G(V, E)$ with pixel coordinates (x, y) as vertices. $img(x, y)$ is the function that maps pixel coordinates to intensity values. The edge relation is also defined as E -

$$\begin{aligned}
img(x, y) > \text{noise} &\implies (x, y) \in V \\
x_2 = x_1 \pm s_x, y_2 = y_1 \pm s_y &\implies ((x_1, y_1), (x_2, y_2)) \in E \\
s_x, s_y \in \{-1, 0, 1\} \\
s_x \neq s_y = 0
\end{aligned}$$

4.2.1 CONNECTED-COMPONENTS and SORT-BY-DISTANCE

The image graph is not necessarily fully connected. By running depth-first-search, the connected components are enlisted into *comps*. Physically, each component represents an indivisible envelope of light intensity. *comps* is sorted by SORT-BY-DISTANCE according to the metric, *m*, which takes a vertex subset, *v*, as its input ($v \in \text{comps}$) -

$$\begin{aligned}
m(v) &= \sqrt{(\bar{x} - x_{img})^2 + (\bar{y} - y_{img})^2} \\
\bar{x} &= \text{mean}(x), \bar{y} = \text{mean}(y) \quad \forall (x, y) \in v
\end{aligned}$$

The metric is essentially the radial pixel distance of the centre of a component, from the centre of the cutout image. This is necessary SDSS catalogs celestial coordinates of *objids* with respect to an object's centre, and any detected peaks should lie in the intensity envelope corresponding to the given *objid*.

4.2.2 FIRST-GROUP and LARGEST-COMPONENT

$$S_i = \{c_j\}, \quad i \in \mathbb{W}$$

$$i = \left\lfloor \frac{m(c_j)}{10} \right\rfloor \forall c_j \in S_i, \quad c_j \in \text{comps}$$

The list $\text{comps} = [c_1, c_2, \dots, c_n]$, sorted by metric $m(v)$, is aggregated into disjoint subsets by the above relation. This contrasts two opposing factors - closeness of an envelope of intensity from the centre of the image, and the relative size of such an envelope. From manual observation of the image samples, it is noted that the underlying image graph is usually disconnected (*true of noisy images*) and it would be remiss to simply choose the closest component to the centre. FIRST-GROUP returns the set S_m where m is the smallest number such that $S_m \neq \emptyset$ and LARGEST-COMPONENT returns the largest component in S_m which is $\max(|c_i|)$, $c_i \in S_m$, which is then stored in $lcmp$

4.2.3 FIND-PEAKS-IN and SORT-BY-INTENSITY

The procedure FIND-PEAKS-IN returns $\text{peak_list} \cap lcmp$ as they are both sets of the form $\{(x, y)\}$. This is stored in pks and any $\text{img}(x, y) < \text{signal}$ for $(x, y) \in \text{pks}$ is discarded by FILTER-BY-INTENSITY. Based on the length of the remaining list, the verdict of SINGLE, DOUBLE or NO_PEAK is returned.

5 Preliminary Detections

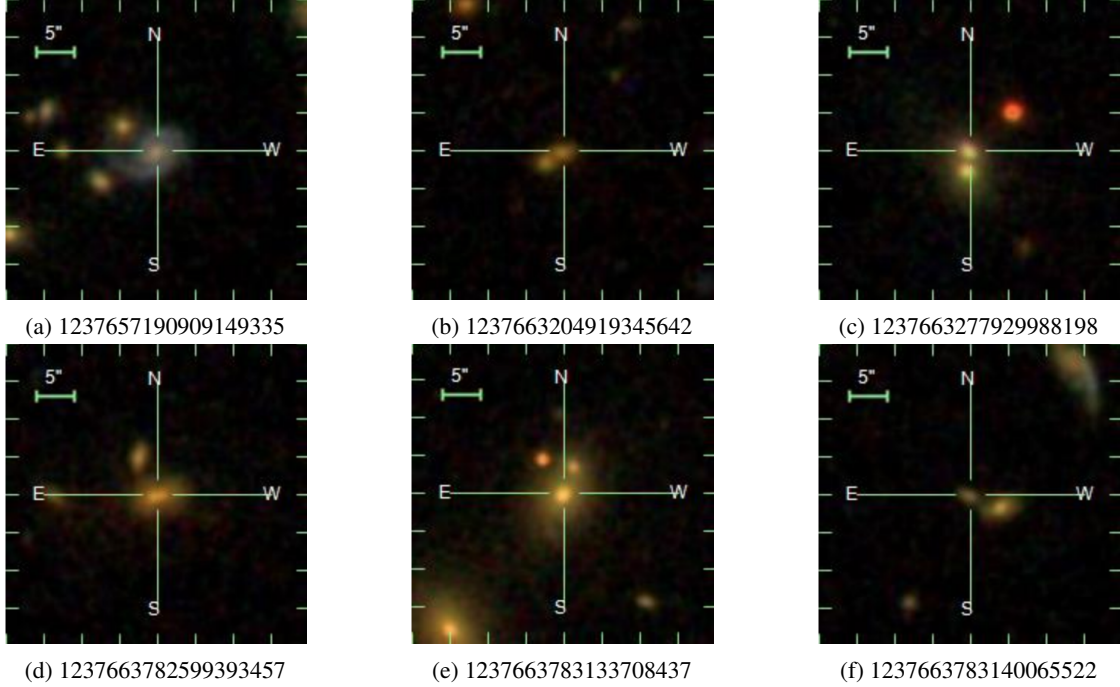


Figure 4: Detections from Blind-Search in Stripe-82

With CasJobs, 100,000 galaxies were chosen at random from the Stripe-82 [2] region and classified by GOTHIC in 4 bands (ugri). The input file is `SDSS_Strip82_100000.csv` (section 2.2). We present some positive detections that also have spectroscopic data available in SDSS. From their cutout images, it can be seen that their morphology is similar to that of NGC-3758 or MRK-212, from the Gimeno sampling. These are displayed in figure (4). Samples such as 4b, 4c, 4e have their double peaks in the same envelope of light. In all probability, these are true double-nuclei galaxies. The remaining 4a, 4d, 4f are two separate, interacting galaxies.

5.1 Blind-Searching in Stripe-82

1. 2,298 galaxies were classified as double-nuclei. These were checked manually for the presence of large foreground stars as SDSS cataloguing is not error free

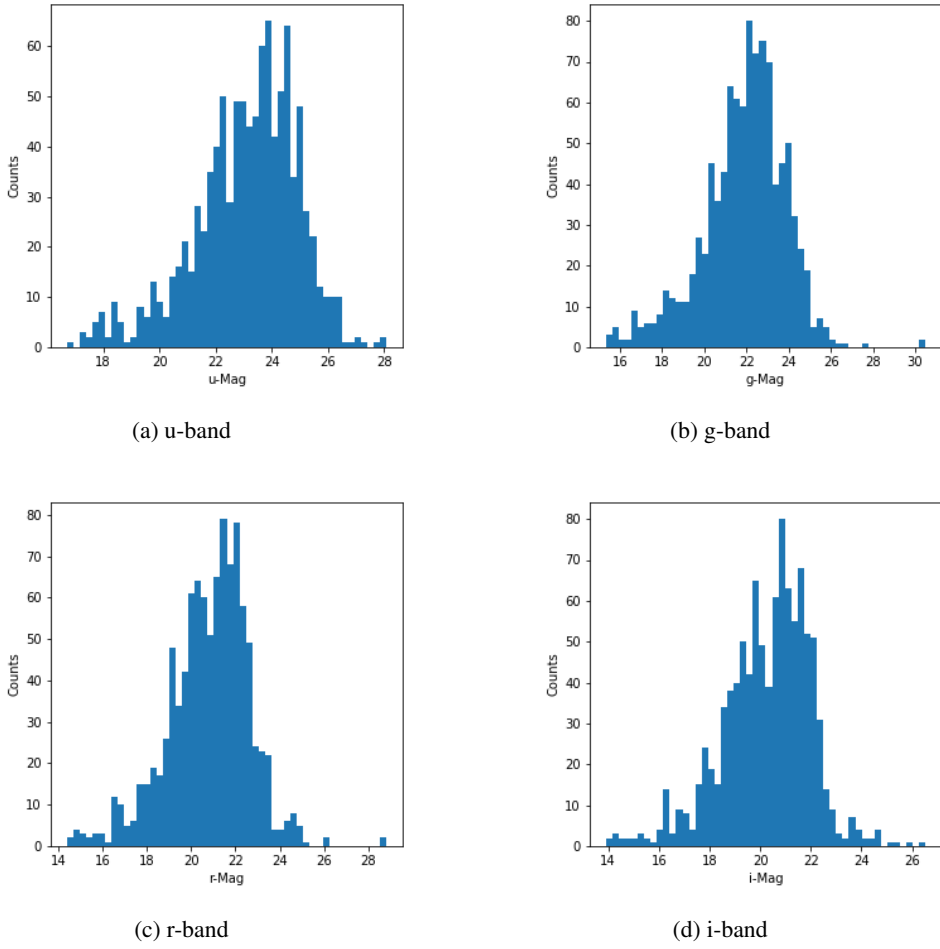


Figure 5: Photometric Magnitudes Distribution in the Stripe-82 Blind-Search

2. 1,246 images were determined to not be dominated by a large foreground star. It was noted that the images from the z-band were extremely noisy/erratic
3. 854 images had valid entries of photometric redshift at both the detected peaks. Of these 589 galaxies had their double peaks cataloged as unique objid in SDSS, and the remaining 206 had non-identical objid among the their two peaks
4. 104 of the 854 had spectral information available

The results from the blind-search are available in `SDSS_Stripe82_Results.csv` (section 2.2). The distributions of the photometric redshifts and the color diagram of the detected double-nuclei galaxies is given in figure (6). The peak is at $z = 0.356$ with a standard deviation of $\sigma_z = 0.197$, and the Kolmogorov-Smirnov goodness-of-fit test gives a statistic of ≈ 0.05 and p-value of ≈ 0.012 . The distribution of the photometric magnitudes in each of the bands is also given in figure (5).

5.1.1 Band Statistics

The maximum simultaneous detection of a double-peaked galaxy was in 4 bands. The maximum detections occurred in the i-band with 519 detections. Detection counts and correlations are summarised in table (1) and (2), respectively.

5.1.2 Detection Accuracy

The false-positive rate is $\frac{2298-854}{2298} \times 100 \approx 62.8\%$. The false negative rate is expected to be minimal as GOTHIC was tested to have 100% accuracy on the Gimeno [20] sample. The high false-positive rate is due to the obstruction of the

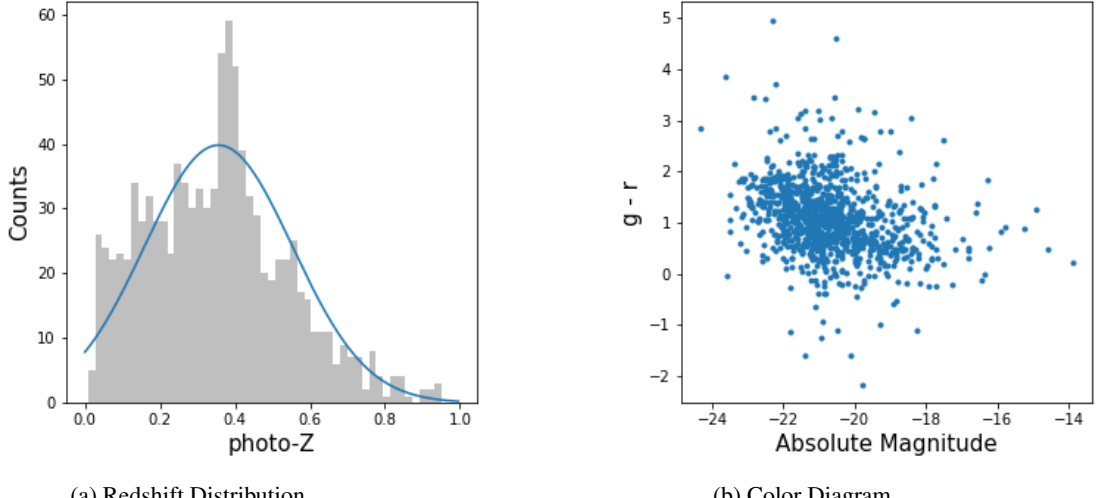


Figure 6: Distributions from Blind-Search in Stripe-82

field of view by large foreground stars in SDSS images, and also due to the fact that SDSS labels of Star/Galaxy are faulty.

Bands	u	g	r	i
Total Detections	90	94	284	519
Exclusive Detections	76	37	140	390
Maximally Correlating Band	i	g	i	r
Detections with above	10	53	123	123

Table 1: Detection information from Blind-Search

Bands	u	g	r	i
u		8	8	10
g	8		53	35
r	8	53		132
i	10	35	132	

Table 2: Band Correlation in Blind-Search

5.2 Cross-Matching SDSS with Gaia

In an effort to reduce the false-positive rate, it was decided to crossmatch the SDSS catalog with Gaia in the Stripe-82 regions. By this method, we have sampled another 100,415 galaxies that are devoid of any stars upto $70''$. To illustrate how interspersed Gaia stars are among the SDSS galaxies, each galaxy in from SDSS is crossmatched to its nearest star in Gaia. Subsequently, the galaxies are binned, according to the angular distance of the nearest crossmatch, in intervals of 10 arcseconds. The resulting plot for the Stripe-82 region is as shown in figure (7). It was done by the KD-Tree crossmatching utility in `astropy`. The input file is `SDSSxGaia_Strip82_100434.csv` (section 2.2)

1. 4,215 galaxies were classified as double-nuclei by GOTHIC
2. 3,573 images were determined to not be dominated by a large foreground star.
3. 3,431 images had valid entries of photometric redshift at both the detected peaks. 3,185 had unique `objid` in SDSS, and 246 were non-identical.
4. 230 had spectral information available

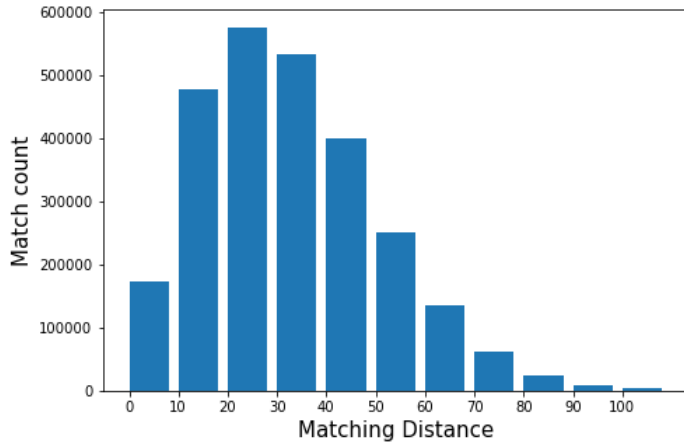


Figure 7: Contamination of SDSS galaxies with Gaia stars in Stripe-82 (X-axis : arcsecond)

5.2.1 Plots and Distributions

The results from the crossmatched search are available in `SDSSxGaia_Stripe82_Results.csv` (section 2.2). The $photoZ$ distribution has nearly the same features as that of the random-search example - a normal distribution with mean at $z = 0.38$ and $\sigma_z = 0.184$. Due to a higher number of galaxies with spectral information available, we have shown the distribution of the schlegel[8] redshift and the color-diagram for the 230 samples in figure (8). The redshift distribution does not have a clear peak, as in the previous case, and the data points in the color-diagram are not as diverse. Double-Nuclei galaxies with spectroscopic data would be necessary to conduct astrophysical studies, and this has been discussed in section (6).

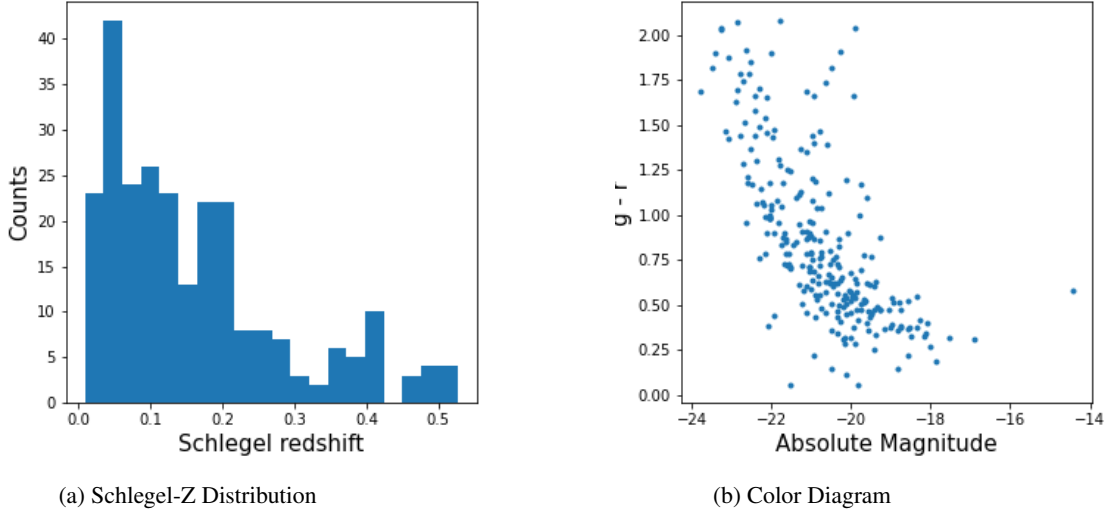


Figure 8: Distributions from Crossmatched-Search in Stripe-82

5.2.2 Band Statistics

The maximum simultaneous detection of a double-peaked galaxy was in 3 bands. The maximum detections occurred in the r-band with 1535 detections. Detection counts and correlations are summarised in table (3) and (4), respectively.

Bands	u	g	r	i
Total Detections	188	441	1535	1472
Exclusive Detections	181	374	1363	1327
Maximally Correlating Band	u	r	i	r
Detections with above	3	54	134	134

Table 3: Detection information from Crossmatched-Search

Bands	u	g	r	i
u		3	3	2
g	3		54	28
r	3	54		134
i	2	28	134	

Table 4: Band Correlation in Crossmatched-Search

5.2.3 Detection Accuracy

The results from random-search and crossmatching with Gaia is summarised in table (5). NDFS is the number of detections that are not dominated by a large foreground star, which is significantly higher in the case of crossmatching. The false positive rate is reduced by 82% and the filtered detection rate (*double peaks that correspond to a valid objid in SDSS*) is increased by 320%

	Random-Search	Gaia-Crossmatch
Input Size	100,000	100,415
GOTHIC Detections	2298	4214
NDFS	854	3753
False-Positive Rate	63%	11%
Filtered Detection Rate	7.95×10^{-3}	3.34×10^{-2}

Table 5: Comparison of Blind and Crossmatched Searches

(NDFS - Not Dominated by Foreground Star)

6 Future Scope of Work

The photoZ attribute in SDSS is itself constructed from predictive techniques[14, 12] and does not provide a strong basis for the astrophysical study of any sample of double-nuclei galaxies obtained via the pipeline. Galaxies with available spectroscopic data would be crucial to further studies and new techniques need to be developed to obtain such sample quickly, as only a tiny fraction of galaxies in SDSS have spectral data available. It would also be useful to develop a technique to differentiate between truly double-nuclei galaxies and interacting galaxies, as demonstrated in figure (4)

7 Conclusion and Summary

A novel detection pipeline GOTHIC, has been proposed, that given an image of a galaxy from SDSS, determines whether it is possibly a double-nuclei galaxy. It enjoys 100% accuracy in the Gimeno[20] sample of double-nuclei galaxies. Focusing on the Stripe-82 region in SDSS, we have sampled 100,000 galaxies at random and run it through the pipeline. Due to a high false-positive rate by the obstruction of foreground stars in the field of view, an alternative cross-matching technique has been used to intelligently sample the input sources, and its superiority has been demonstrated by its higher detection and lower false-positive rate.

8 Acknowledgements

The first author gratefully acknowledges the support received from the Indian Institute of Astrophysics, Bangalore, India during an internship. The second author would like to thank the Science and Engineering research Board (SERB), Department of Science and Technology, Government of India, for supporting our research by providing us with resources to conduct our experiments. The project reference number is: EMR/2016/005687.

Funding for the SDSS and SDSS-II has been provided by the Alfred P. Sloan Foundation, the Participating Institutions, the National Science Foundation, the U.S. Department of Energy, the National Aeronautics and Space Administration, the Japanese Monbukagakusho, the Max Planck Society, and the Higher Education Funding Council for England. The SDSS Web Site is <http://www.sdss.org/>. The SDSS is managed by the Astrophysical Research Consortium for the Participating Institutions. The Participating Institutions are the American Museum of Natural History, Astrophysical Institute Potsdam, University of Basel, University of Cambridge, Case Western Reserve University, University of Chicago, Drexel University, Fermilab, the Institute for Advanced Study, the Japan Participation Group, Johns Hopkins University, the Joint Institute for Nuclear Astrophysics, the Kavli Institute for Particle Astrophysics and Cosmology, the Korean Scientist Group, the Chinese Academy of Sciences (LAMOST), Los Alamos National Laboratory, the Max-Planck- Institute for Astronomy (MPIA), the Max-Planck-Institute for Astrophysics (MPA), New Mexico State University, Ohio State University, University of Pittsburgh, University of Portsmouth, Princeton University, the United States Naval Observatory, and the University of Washington.

References

- [1] Maan H. , Hayman Gosain, Sara L. Ellison, David R. Patton, and Paul Torrey. Interacting galaxies in the IllustrisTNG simulations - II: star formation in the post-merger stage. *Monthly Notices of the Royal Astronomical Society*, 493(3):3716–3731, apr 2020.
- [2] Kevork N. Abazajian, Jennifer K. Adelman-McCarthy, Marcel A. Agüeros, Sahar S. Allam, Carlos Allende Prieto, Deokkeun An, Kurt S. J. Anderson, Scott F. Anderson, James Annis, Neta A. Bahcall, C. A. L. Bailer-Jones, J. C. Barentine, Bruce A. Bassett, Andrew C. Becker, Timothy C. Beers, Eric F. Bell, Vasily Belokurov, Andreas A. Berlind, Eileen F. Berman, Mariangela Bernardi, Steven J. Bickerton, Dmitry Bizyaev, John P. Blakeslee, Michael R. Blanton, John J. Bochanski, William N. Boroski, Howard J. Brewington, Jarle Brinchmann, J. Brinkmann, Robert J. Brunner, Tamás Budavári, Larry N. Carey, Samuel Carliles, Michael A. Carr, Francisco J. Castander, David Cinabro, A. J. Connolly, István Csabai, Carlos E. Cunha, Paul C. Czarapata, James R. A. Davenport, Ernst de Haas, Ben Dilday, Mamoru Doi, Daniel J. Eisenstein, Michael L. Evans, N. W. Evans, Xiaohui Fan, Scott D. Friedman, Joshua A. Frieman, Masataka Fukugita, Boris T. Gänsicke, Evalyn Gates, Bruce Gillespie, G. Gilmore, Belinda Gonzalez, Carlos F. Gonzalez, Eva K. Grebel, James E. Gunn, Zsuzsanna Györy, Patrick B. Hall, Paul Harding, Frederick H. Harris, Michael Harvanek, Suzanne L. Hawley, Jeffrey J. E. Hayes, Timothy M. Heckman, John S. Hendry, Gregory S. Hennessy, Robert B. Hindsley, J. Hoblitt, Craig J. Hogan, David W. Hogg, Jon A. Holtzman, Joseph B. Hyde, Shin ichi Ichikawa, Takashi Ichikawa, Myung-shin Im, Željko Ivezić, Sebastian Jester, Linhua Jiang, Jennifer A. Johnson, Anders M. Jorgensen, Mario Jurić, Stephen M. Kent, R. Kessler, S. J. Kleinman, G. R. Knapp, Kohki Konishi, Richard G. Kron, Jurek Krzesinski, Nikolay Kuropatkin, Hubert Lampeitl, Svetlana Lebedeva, Myung Gyoong Lee, Young Sun Lee, R. French Leger, Sébastien Lépine, Nolan Li, Marcos Lima, Huan Lin, Daniel C. Long, Craig P. Loomis, Jon Loveday, Robert H. Lupton, Eugene Magnier, Olena Malanushenko, Viktor Malanushenko, Rachel Mandelbaum, Bruce Margon, John P. Marriner, David Martínez-Delgado, Takahiko Matsubara, Peregrine M. McGehee, Timothy A. McKay, Avery Meiksin, Heather L. Morrison, Fergal Mullally, Jeffrey A. Munn, Tara Murphy, Thomas Nash, Ada Nebot, Eric H. Neilsen, Heidi Jo Newberg, Peter R. Newman, Robert C. Nichol, Tom Nicinski, Maria Nieto-Santisteban, Atsuko Nitta, Sadanori Okamura, Daniel J. Oravetz, Jeremiah P. Ostriker, Russell Owen, Nikhil Padmanabhan, Kaike Pan, Changbom Park, George Pauls, John Peoples, Will J. Percival, Jeffrey R. Pier, Adrian C. Pope, Dimitri Pourbaix, Paul A. Price, Norbert Purger, Thomas Quinn, M. Jordan Raddick, Paola Re Fiorentin, Gordon T. Richards, Michael W. Richmond, Adam G. Riess, Hans-Walter Rix, Constance M. Rockosi, Masao Sako, David J. Schlegel, Donald P. Schneider, Ralf-Dieter Scholz, Matthias R. Schreiber, Axel D. Schwipe, Uroš Seljak, Branimir Sesar, Erin Sheldon, Kazu Shimasaku, Valena C. Sibley, A. E. Simmons, Thirupathi Sivarani, J. Allyn Smith, Martin C. Smith, Vernesa Smolčić, Stephanie A. Snedden, Albert Stebbins, Matthias Steinmetz, Chris Stoughton, Michael A. Strauss, Mark SubbaRao, Yasushi Suto, Alexander S. Szalay, István Szapudi, Paula Szkody, Masayuki Tanaka, Max Tegmark, Luis F. A. Teodoro, Aniruddha R. Thakar, Christy A. Tremonti, Douglas L. Tucker, Alan Uomoto, Daniel E. Vanden Berk, Jan Vandenberg, S. Vidrih, Michael S. Vogeley, Wolfgang Voges, Nicole P. Vogt, Yogesh Wadadekar, Shannon Watters, David H. Weinberg, Andrew A. West, Simon D. M. White, Brian C. Wilhite, Alainna C. Wonders, Brian Yanny, D. R. Yocom, Donald G. York, Idit Zehavi, Stefano Zibetti, and Daniel B. Zucker. The Seventh Data Release of the Sloan Digital Sky Survey. *The Astrophysical Journal Supplement Series*, 182(2):543–558, may 2009.
- [3] B. P. Abbott, R. Abbott, T. D. Abbott, M. R. Abernathy, F. Acernese, K. Ackley, C. Adams, T. Adams, P. Adesso, R. X. Adhikari, V. B. Adya, C. Affeldt, M. Agathos, K. Agatsuma, N. Aggarwal, O. D. Aguiar, L. Aiello, A. Ain, P. Ajith, B. Allen, A. Allocca, P. A. Altin, S. B. Anderson, W. G. Anderson, K. Arai, M. A. Arain, M. C. Araya, C. C. Arceneaux, J. S. Areeda, N. Arnaud, K. G. Arun, S. Ascenzi, G. Ashton, M. Ast, S. M. Aston, P. Astone, P. Aufmuth, C. Aulbert, S. Babak, P. Bacon, M. K. M. Bader, P. T. Baker, F. Baldaccini, G. Ballardin,

S. W. Ballmer, J. C. Barayoga, S. E. Barclay, B. C. Barish, D. Barker, F. Barone, B. Barr, L. Barsotti, M. Barsuglia, D. Barta, J. Bartlett, M. A. Barton, I. Bartos, R. Bassiri, A. Basti, J. C. Batch, C. Baune, V. Bavigadda, M. Bazzan, B. Behnke, M. Bejger, C. Belczynski, A. S. Bell, C. J. Bell, B. K. Berger, J. Bergman, G. Bergmann, C. P. L. Berry, D. Bersanetti, A. Bertolini, J. Betzwieser, S. Bhagwat, R. Bhandare, I. A. Bilenko, G. Billingsley, J. Birch, R. Birney, O. Birnholtz, S. Biscans, A. Bisht, M. Bitossi, C. Biwer, M. A. Bizouard, J. K. Blackburn, C. D. Blair, D. G. Blair, R. M. Blair, S. Bloemen, O. Bock, T. P. Bodiya, M. Boer, G. Bogaert, C. Bogan, A. Bohe, P. Bojtos, C. Bond, F. Bondu, R. Bonnand, B. A. Boom, R. Bork, V. Boschi, S. Bose, Y. Bouffanais, A. Bozzi, C. Bradaschia, P. R. Brady, V. B. Braginsky, M. Branchesi, J. E. Brau, T. Briant, A. Brillet, M. Brinkmann, V. Brisson, P. Brockill, A. F. Brooks, D. A. Brown, D. D. Brown, N. M. Brown, C. C. Buchanan, A. Buikema, T. Bulik, H. J. Bulten, A. Buonanno, D. Buskulic, C. Buy, R. L. Byer, M. Cabero, L. Cadonati, G. Cagnoli, C. Cahillane, J. Calderón Bustillo, T. Callister, E. Calloni, J. B. Camp, K. C. Cannon, J. Cao, C. D. Capano, E. Capocasa, F. Carbognani, S. Caride, J. Casanueva Diaz, C. Casentini, S. Caudill, M. Cavaglià, F. Cavalier, R. Cavalieri, G. Cella, C. B. Cepeda, L. Cerboni Baiardi, G. Cerretani, E. Cesarini, R. Chakraborty, T. Chalermongsak, S. J. Chamberlin, M. Chan, S. Chao, P. Charlton, E. Chassande-Mottin, H. Y. Chen, Y. Chen, C. Cheng, A. Chincarini, A. Chiummo, H. S. Cho, M. Cho, J. H. Chow, N. Christensen, Q. Chu, S. Chua, S. Chung, G. Ciani, F. Clara, J. A. Clark, F. Cleva, E. Coccia, P.-F. Cohadon, A. Colla, C. G. Collette, L. Cominsky, M. Constancio, A. Conte, L. Conti, D. Cook, T. R. Corbitt, N. Cornish, A. Corsi, S. Cortese, C. A. Costa, M. W. Coughlin, S. B. Coughlin, J.-P. Coulon, S. T. Countryman, P. Couvares, E. E. Cowan, D. M. Coward, M. J. Cowart, D. C. Coyne, R. Coyne, K. Craig, J. D. E. Creighton, T. D. Creighton, J. Cripe, S. G. Crowder, A. M. Cruise, A. Cumming, L. Cunningham, E. Cuoco, T. Dal Canton, S. L. Danilishin, S. D'Antonio, K. Danzmann, N. S. Darman, C. F. Da Silva Costa, V. Dattilo, I. Dave, H. P. Daveloza, M. Davier, G. S. Davies, E. J. Daw, R. Day, S. De, D. DeBra, G. Debreczeni, J. Degallaix, M. De Laurentis, S. Deléglise, W. Del Pozzo, T. Denker, T. Dent, H. Dereli, V. Dergachev, R. T. DeRosa, R. De Rosa, R. DeSalvo, S. Dhurandhar, M. C. Díaz, L. Di Fiore, M. Di Giovanni, A. Di Lieto, S. Di Pace, I. Di Palma, A. Di Virgilio, G. Dojcinoski, V. Dolique, F. Donovan, K. L. Dooley, S. Doravari, R. Douglas, T. P. Downes, M. Drago, R. W. P. Drever, J. C. Driggers, Z. Du, M. Ducrot, S. E. Dwyer, T. B. Edo, M. C. Edwards, A. Effler, H.-B. Eggenstein, P. Ehrens, J. Eichholz, S. S. Eikenberry, W. Engels, R. C. Essick, T. Etzel, M. Evans, T. M. Evans, R. Everett, M. Factourovich, V. Fafone, H. Fair, S. Fairhurst, X. Fan, Q. Fang, S. Farinon, B. Farr, W. M. Farr, M. Favata, M. Fays, H. Fehrmann, M. M. Fejer, D. Feldbaum, I. Ferrante, E. C. Ferreira, F. Ferrini, F. Fidecaro, L. S. Finn, I. Fiori, D. Fiorucci, R. P. Fisher, R. Flaminio, M. Fletcher, H. Fong, J.-D. Fournier, S. Franco, S. Frasca, F. Frasconi, M. Frede, Z. Frei, A. Freise, R. Frey, V. Frey, T. T. Fricke, P. Fritschel, V. V. Frolov, P. Fulda, M. Fyffe, H. A. G. Gabbard, J. R. Gair, L. Gammaitoni, S. G. Gaonkar, F. Garufi, A. Gatto, G. Gaur, N. Gehrels, G. Gemme, B. Gendre, E. Genin, A. Gennai, J. George, L. Gergely, V. Germain, Abhirup Ghosh, Archisman Ghosh, S. Ghosh, J. A. Giaime, K. D. Giardina, A. Giazotto, K. Gill, A. Glaefke, J. R. Gleason, E. Goetz, R. Goetz, L. Gondan, G. González, J. M. Gonzalez Castro, A. Gopakumar, N. A. Gordon, M. L. Gorodetsky, S. E. Gossan, M. Gosselin, R. Gouaty, C. Graef, P. B. Graff, M. Granata, A. Grant, S. Gras, C. Gray, G. Greco, A. C. Green, R. J. S. Greenhalgh, P. Groot, H. Grote, S. Grunewald, G. M. Guidi, X. Guo, A. Gupta, M. K. Gupta, K. E. Gushwa, E. K. Gustafson, R. Gustafson, J. J. Hacker, B. R. Hall, E. D. Hall, G. Hammond, M. Haney, M. M. Hanke, J. Hanks, C. Hanna, M. D. Hannam, J. Hanson, T. Hardwick, J. Harms, G. M. Harry, I. W. Harry, M. J. Hart, M. T. Hartman, C.-J. Haster, K. Haughian, J. Healy, J. Heefner, A. Heidmann, M. C. Heintze, G. Heinzel, H. Heitmann, P. Hello, G. Hemming, M. Hendry, I. S. Heng, J. Hennig, A. W. Heptonstall, M. Heurs, S. Hild, D. Hoak, K. A. Hodge, D. Hofman, S. E. Hollitt, K. Holt, D. E. Holz, P. Hopkins, D. J. Hosken, J. Hough, E. A. Houston, E. J. Howell, Y. M. Hu, S. Huang, E. A. Huerta, D. Huet, B. Hughey, S. Husa, S. H. Huttner, T. Huynh-Dinh, A. Idrisy, N. Indik, D. R. Ingram, R. Inta, H. N. Isa, J.-M. Isac, M. Isi, G. Islas, T. Isogai, B. R. Iyer, K. Izumi, M. B. Jacobson, T. Jacqmin, H. Jang, K. Jani, P. Jaranowski, S. Jawahar, F. Jiménez-Forteza, W. W. Johnson, N. K. Johnson-McDaniel, D. I. Jones, R. Jones, R. J. G. Jonker, L. Ju, K. Haris, C. V. Kalaghatgi, V. Kalogera, S. Kandhasamy, G. Kang, J. B. Kanner, S. Karki, M. Kasprzack, E. Katsavounidis, W. Katzman, S. Kaufer, T. Kaur, K. Kawabe, F. Kawazoe, F. Kéfélian, M. S. Kehl, D. Keitel, D. B. Kelley, W. Kells, R. Kennedy, D. G. Keppel, J. S. Key, A. Khalaidovski, F. Y. Khalil, I. Khan, S. Khan, Z. Khan, E. A. Khazanov, N. Kijbunchoo, C. Kim, J. Kim, K. Kim, Nam-Gyu Kim, Namjun Kim, Y.-M. Kim, E. J. King, P. J. King, D. L. Kinzel, J. S. Kissel, L. Kleybolte, S. Klimenko, S. M. Koehlenbeck, K. Kokeyama, S. Koley, V. Kondrashov, A. Kontos, S. Koranda, M. Korobko, W. Z. Korth, I. Kowalska, D. B. Kozak, V. Kringsel, B. Krishnan, A. Królak, C. Krueger, G. Kuehn, P. Kumar, R. Kumar, L. Kuo, A. Kutytnia, P. Kwee, B. D. Lackey, M. Landry, J. Lange, B. Lantz, P. D. Lasky, A. Lazzarini, C. Lazzaro, P. Leaci, S. Leavey, E. O. Lebigot, C. H. Lee, H. K. Lee, H. M. Lee, K. Lee, A. Lennon, M. Leonardi, J. R. Leong, N. Leroy, N. Letendre, Y. Levin, B. M. Levine, T. G. F. Li, A. Libson, T. B. Littenberg, N. A. Lockerbie, J. Logue, A. L. Lombardi, L. T. London, J. E. Lord, M. Lorenzini, V. Loriette, M. Lormand, G. Losurdo, J. D. Lough, C. O. Lousto, G. Lovelace, H. Lück, A. P. Lundgren, J. Luo, R. Lynch, Y. Ma, T. MacDonald, B. Machenschalk, M. MacInnis, D. M. Macleod, F. Magaña Sandoval, R. M. Magee, M. Mageswaran, E. Majorana, I. Maksimovic, V. Malvezzi, N. Man, I. Mandel, V. Mandic, V. Mangano, G. L. Mansell, M. Manske, M. Mantovani, F. March-

esoni, F. Marion, S. Márka, Z. Márka, A. S. Markosyan, E. Maros, F. Martelli, L. Martellini, I. W. Martin, R. M. Martin, D. V. Martynov, J. N. Marx, K. Mason, A. Masserot, T. J. Massinger, M. Masso-Reid, F. Matichard, L. Matone, N. Mavalvala, N. Mazumder, G. Mazzolo, R. McCarthy, D. E. McClelland, S. McCormick, S. C. McGuire, G. McIntyre, J. McIver, D. J. McManus, S. T. McWilliams, D. Meacher, G. D. Meadors, J. Meidam, A. Melatos, G. Mendell, D. Mendoza-Gandara, R. A. Mercer, E. Merilh, M. Merzougui, S. Meshkov, C. Messenger, C. Messick, P. M. Meyers, F. Mezzani, H. Miao, C. Michel, H. Middleton, E. E. Mikhailov, L. Milano, J. Miller, M. Millhouse, Y. Minenkov, J. Ming, S. Mirshekari, C. Mishra, S. Mitra, V. P. Mitrofanov, G. Mitselmakher, R. Mittleman, A. Moggi, M. Mohan, S. R. P. Mohapatra, M. Montani, B. C. Moore, C. J. Moore, D. Moraru, G. Moreno, S. R. Morriss, K. Mossavi, B. Mouris, C. M. Mow-Lowry, C. L. Mueller, G. Mueller, A. W. Muir, Arunava Mukherjee, D. Mukherjee, S. Mukund, A. Mullavey, J. Munch, D. J. Murphy, P. G. Murray, A. Mytidis, I. Nardecchia, L. Naticchioni, R. K. Nayak, V. Necula, K. Nedkova, G. Nelemans, M. Neri, A. Neunzert, G. Newton, T. T. Nguyen, A. B. Nielsen, S. Nissanke, A. Nitz, F. Nocera, D. Nolting, M. E. N. Normandin, L. K. Nuttall, J. Oberling, E. Ochsner, J. O'Dell, E. Oelker, G. H. Ogin, J. J. Oh, S. H. Oh, F. Ohme, M. Oliver, P. Oppermann, Richard J. Oram, B. O'Reilly, R. O'Shaughnessy, C. D. Ott, D. J. Ottaway, R. S. Ottens, H. Overmier, B. J. Owen, A. Pai, S. A. Pai, J. R. Palamos, O. Palashov, C. Palomba, A. Pal-Singh, H. Pan, Y. Pan, C. Pankow, F. Pannarale, B. C. Pant, F. Paoletti, A. Paoli, M. A. Papa, H. R. Paris, W. Parker, D. Pascucci, A. Pasqualetti, R. Passaquieti, D. Passuello, B. Patricelli, Z. Patrick, B. L. Pearlstone, M. Pedraza, R. Pedurand, L. Pekowsky, A. Pele, S. Penn, A. Perreca, H. P. Pfeiffer, M. Phelps, O. Piccinni, M. Pichot, M. Pickenpack, F. Piergiovanni, V. Pierro, G. Pillant, L. Pinard, I. M. Pinto, M. Pitkin, J. H. Poeld, R. Poggiani, P. Popolizio, A. Post, J. Powell, J. Prasad, V. Predoi, S. S. Premachandra, T. Prestegard, L. R. Price, M. Prijatelj, M. Principe, S. Privitera, R. Prix, G. A. Prodi, L. Prokhorov, O. Puncken, M. Punturo, P. Puppo, M. Pürer, H. Qi, J. Qin, V. Quetschke, E. A. Quintero, R. Quitzow-James, F. J. Raab, D. S. Rabeling, H. Radkins, P. Raffai, S. Raja, M. Rakhmanov, C. R. Ramet, P. Rapagnani, V. Raymond, M. Razzano, V. Re, J. Read, C. M. Reed, T. Regimbau, L. Rei, S. Reid, D. H. Reitze, H. Rew, S. D. Reyes, F. Ricci, K. Riles, N. A. Robertson, R. Robie, F. Robinet, A. Rocchi, L. Rolland, J. G. Rollins, V. J. Roma, J. D. Romano, R. Romano, G. Romanov, J. H. Romie, D. Rosińska, S. Rowan, A. Rüdiger, P. Ruggi, K. Ryan, S. Sachdev, T. Sadecki, L. Sadeghian, L. Salconi, M. Saleem, F. Salemi, A. Samajdar, L. Sammut, L. M. Sampson, E. J. Sanchez, V. Sandberg, B. Sandeen, G. H. Sanders, J. R. Sanders, B. Sassolas, B. S. Sathyaprakash, P. R. Saulson, O. Sauter, R. L. Savage, A. Sawadsky, P. Schale, R. Schilling, J. Schmidt, P. Schmidt, R. Schnabel, R. M. S. Schofield, A. Schönbeck, E. Schreiber, D. Schuette, B. F. Schutz, J. Scott, S. M. Scott, D. Sellers, A. S. Sengupta, D. Sentenac, V. Sequino, A. Sergeev, G. Serna, Y. Setyawati, A. Sevigny, D. A. Shaddock, T. Shaffer, S. Shah, M. S. Shahriar, M. Shaltev, Z. Shao, B. Shapiro, P. Shawhan, A. Sheperd, D. H. Shoemaker, D. M. Shoemaker, K. Siellez, X. Siemens, D. Sigg, A. D. Silva, D. Simakov, A. Singer, L. P. Singer, A. Singh, R. Singh, A. Singhal, A. M. Sintes, B. J. J. Slagmolen, J. R. Smith, M. R. Smith, N. D. Smith, R. J. E. Smith, E. J. Son, B. Sorazu, F. Sorrentino, T. Souradeep, A. K. Srivastava, A. Staley, M. Steinke, J. Steinlechner, S. Steinlechner, D. Steinmeyer, B. C. Stephens, S. P. Stevenson, R. Stone, K. A. Strain, N. Straniero, G. Stratta, N. A. Strauss, S. Strigin, R. Sturani, A. L. Stuver, T. Z. Summerscales, L. Sun, P. J. Sutton, B. L. Swinkels, M. J. Szczepańczyk, M. Tacca, D. Talukder, D. B. Tanner, M. Tápai, S. P. Tarabrin, A. Taracchini, R. Taylor, T. Theeg, M. P. Thirugnanasambandam, E. G. Thomas, M. Thomas, P. Thomas, K. A. Thorne, K. S. Thorne, E. Thrane, S. Tiwari, V. Tiwari, K. V. Tokmakov, C. Tomlinson, M. Tonelli, C. V. Torres, C. I. Torrie, D. Töyrä, F. Travasso, G. Traylor, D. Trifirò, M. C. Tringali, L. Trozzo, M. Tse, M. Turconi, D. Tuyenbayev, D. Ugolini, C. S. Unnikrishnan, A. L. Urban, S. A. Usman, H. Vahlbruch, G. Vajente, G. Valdes, M. Vallisneri, N. van Bakel, M. van Beuzekom, J. F. J. van den Brand, C. Van Den Broeck, D. C. Vander-Hyde, L. van der Schaaf, J. V. van Heijningen, A. A. van Veggel, M. Vardaro, S. Vass, M. Vasúth, R. Vaulin, A. Vecchio, G. Vedovato, J. Veitch, P. J. Veitch, K. Venkateswara, D. Verkindt, F. Vetrano, A. Viceré, S. Vinciguerra, D. J. Vine, J.-Y. Vinet, S. Vitale, T. Vo, H. Vocca, C. Vorick, D. Voss, W. D. Vousden, S. P. Vyatchanin, A. R. Wade, L. E. Wade, M. Wade, S. J. Waldman, M. Walker, L. Wallace, S. Walsh, G. Wang, H. Wang, M. Wang, X. Wang, Y. Wang, H. Ward, R. L. Ward, J. Warner, M. Was, B. Weaver, L.-W. Wei, M. Weinert, A. J. Weinstein, R. Weiss, T. Welborn, L. Wen, P. Weßels, T. Westphal, K. Wette, J. T. Whelan, S. E. Whitcomb, D. J. White, B. F. Whiting, K. Wiesner, C. Wilkinson, P. A. Willems, L. Williams, R. D. Williams, A. R. Williamson, J. L. Willis, B. Willke, M. H. Wimmer, L. Winkelmann, W. Winkler, C. C. Wipf, A. G. Wiseman, H. Wittel, G. Woan, J. Worden, J. L. Wright, G. Wu, J. Yablon, I. Yakushin, W. Yam, H. Yamamoto, C. C. Yancey, M. J. Yap, H. Yu, M. Yvert, A. Zadrożny, L. Zangrandi, M. Zanolin, J.-P. Zendri, M. Zevin, F. Zhang, L. Zhang, M. Zhang, Y. Zhang, C. Zhao, M. Zhou, Z. Zhou, X. J. Zhu, M. E. Zucker, S. E. Zuraw, and J. Zweizig. Observation of gravitational waves from a binary black hole merger. *Phys. Rev. Lett.*, 116:061102, Feb 2016.

[4] L. Ballo, V. Braito, R. Della Ceca, L. Maraschi, F. Tavecchio, and M. Dadina. Arp 299: a second merging system with two active nuclei? *Nuclear Physics B - Proceedings Supplements*, 132:141 – 144, 2004. Proceedings of the 2nd BeppoSAX Conference: The Restless High-Energy Universe.

[5] Joshua E. Barnes and Lars Hernquist. Dynamics of interacting galaxies. *Annual Review of Astronomy and Astrophysics*, 30:705–742, jan 1992.

[6] Stefano Bianchi, Marco Chiaberge, Enrico Piconcelli, Matteo Guainazzi, and Giorgio Matt. Chandra unveils a binary active galactic nucleus in Mrk 463. *Monthly Notices of the Royal Astronomical Society*, 386(1):105–110, 03 2008.

[7] Kelly A. Blumenthal, Jorge Moreno, Joshua E. Barnes, Lars Hernquist, Paul Torrey, Zachary Claytor, Vicente Rodriguez-Gomez, Federico Marinacci, and Mark Vogelsberger. Galaxy interactions in IllustrisTNG-100, I: The power and limitations of visual identification. *Monthly Notices of the Royal Astronomical Society*, 492(2):2075–2094, February 2020.

[8] Adam S. Bolton, David J. Schlegel, Éric Aubourg, Stephen Bailey, Vaishali Bhardwaj, Joel R. Brownstein, Scott Burles, Yan Mei Chen, Kyle Dawson, Daniel J. Eisenstein, James E. Gunn, G. R. Knapp, Craig P. Loomis, Robert H. Lupton, Claudia Maraston, Demitri Muna, Adam D. Myers, Matthew D. Olmstead, Nikhil Padmanabhan, Isabelle Pâris, Will J. Percival, Patrick Petitjean, Constance M. Rockosi, Nicholas P. Ross, Donald P. Schneider, Yiping Shu, Michael A. Strauss, Daniel Thomas, Christy A. Tremonti, David A. Wake, Benjamin A. Weaver, and W. Michael Wood-Vasey. Spectral classification and redshift measurement for the sdss-iii baryon oscillation spectroscopic survey. *Astronomical Journal*, 144(5), November 2012.

[9] Gregory D. Bothun, Jules P. Halpern, Carol J. Lonsdale, Chris Impey, and Mark Schmitz. The Wasilewski Sample of Emission-Line Galaxies: Follow-up CCD Imaging and Spectroscopic and IRAS Observations. *The Astrophysical Journal*, 70:271, June 1989.

[10] J. Canny. A computational approach to edge detection. *IEEE Transactions on Pattern Analysis and Machine Intelligence*, PAMI-8(6):679–698, 1986.

[11] N. Caon, M. Capaccioli, and M. D’Onofrio. On the shape of the light profiles of early-type galaxies. *Monthly Notices of the Royal Astronomical Society*, 265(4):1013–1021, 12 1993.

[12] Samuel Carliles, Tamás Budavári, Sébastien Heinis, Carey Priebe, and Alexander S. Szalay. Random Forests for Photometric Redshifts. *The Astrophysical Journal*, 712(1):511–515, mar 2010.

[13] B. A Cook. Acronym: Acronym creation for you and me, 2019.

[14] I. Csabai, L. Dobos, M. Trencséni, G. Herczegh, P. Józsa, N. Purger, T. Budavári, and A.S. Szalay. Multidimensional indexing tools for the virtual observatory. *Astronomische Nachrichten*, 328(8):852–857, 2007.

[15] Mousumi Das, Khatun Rubinur, Preeti Kharb, Ashlin Varghese, Navyasree Novakkuni, and Atul James. Dual Active Galactic Nuclei in Nearby Galaxies. *Bulletin de la Societe Royale des Sciences de Liege*, 87:299–306, April 2018.

[16] Jonathan J. Davies, Robert A. Crain, Benjamin D. Oppenheimer, and Joop Schaye. The quenching and morphological evolution of central galaxies is facilitated by the feedback-driven expulsion of circumgalactic gas. *Monthly Notices of the Royal Astronomical Society*, 491(3):4462–4480, January 2020.

[17] M. Davis, G. Efstathiou, C. S. Frenk, and S. D. M. White. The evolution of large-scale structure in a universe dominated by cold dark matter. *The Astrophysical Journal*, 292:371–394, May 1985.

[18] A. Dressler. The evolution of galaxies in clusters. *Annual Review of Astronomy and Astrophysics*, 22(1):185–222, 1984.

[19] K. É. Gabányi, T. An, S. Frey, S. Komossa, Z. Paragi, X.-Y. Hong, and Z.-Q. Shen. Four Dual AGN Candidates Observed With The VLBA. *The Astrophysical Journal*, 826(2):106, jul 2016.

[20] Germán N. Gimeno, Rubén J. Díaz, and Gustavo J. Carranza. Catalog of double nucleus disk galaxies. *The Astronomical Journal*, 128(1):62–67, jul 2004.

[21] Andy D. Goulding, Kris Pardo, Jenny E. Greene, Chiara M. F. Mingarelli, Kristina Nyland, and Michael A. Strauss. Discovery of a Close-separation Binary Quasar at the Heart of a $z \sim 0.2$ Merging Galaxy and Its Implications for Low-frequency Gravitational Waves. *The Astrophysical Journal*, 879(2):L21, July 2019.

[22] Philip F. Hopkins, Dale D. Kocevski, and Kevin Bundy. Do we expect most AGN to live in discs? *Monthly Notices of the Royal Astronomical Society*, 445(1):823–834, 09 2014.

[23] P. Kharb, D. V. Lal, and D. Merritt. A candidate sub-parsec binary black hole in the Seyfert galaxy NGC 7674. *Nature Astronomy*, 1:727–733, September 2017.

[24] S. Komossa, V. Burwitz, G. Hasinger, P. Predehl, J. S. Kaastra, and Y. Ikebe. Discovery of a Binary Active Galactic Nucleus in the Ultraluminous Infrared Galaxy NGC 6240 Using Chandra. *The Astrophysical Journal*, 582(1):L15–L19, January 2003.

[25] S. Komossa and J. A. Zensus. Compact object mergers: observations of supermassive binary black holes and stellar tidal disruption events. *Proceedings of the International Astronomical Union*, 10(S312):13–25, Aug 2014.

[26] Michael Koss, Richard Mushotzky, Ezequiel Treister, Sylvain Veilleux, Ranjan Vasudevan, and Margaret Trippe. Understanding dual active galactic nucleus activation in the nearby universe. *The Astrophysical Journal*, 746(2):L22, feb 2012.

[27] Michael Koss, Richard Mushotzky, Sylvain Veilleux, Ranjan Vasudevan, Neal Miller, D. B. Sanders, Kevin Schawinski, and Margaret Trippe. Chandra Discovery of a Binary Active Galactic Nucleus in Mrk 739. *The Astrophysical Journal*, 735(2):L42, jun 2011.

[28] M. Mezcua, A. P. Lobanov, E. Mediavilla, and M. Karouzos. Photometric decomposition of mergers in disc galaxies. *The Astrophysical Journal*, 784(1):16, feb 2014.

[29] Hagai Netzer, W. Kollatschny, and K. J. Fricke. Study of multiple nucleus galaxies. II. MKN 739. *Astronomy and Astrophysics*, 171:41–48, January 1987.

[30] David R. Patton, Farid D. Qamar, Sara L. Ellison, Asa F. L. Bluck, Luc Simard, J. Trevor Mendel, Jorge Moreno, and Paul Torrey. Galaxy pairs in the Sloan Digital Sky Survey - XI. A new method for measuring the influence of the closest companion out to wide separations. *Monthly Notices of the Royal Astronomical Society*, 461(3):2589–2604, September 2016.

[31] Bradley M. Peterson. *An Introduction to Active Galactic Nuclei*. 1997.

[32] K. Rubinur, M. Das, and P. Kharb. Searching for dual active galactic nuclei. *Journal of Astrophysics and Astronomy*, 39(1):8, February 2018.

[33] K. Rubinur, M. Das, and P. Kharb. Searching for dual AGN in galaxies with double-peaked emission line spectra using radio observations. *Monthly Notices of the Royal Astronomical Society*, 484(4):4933–4950, April 2019.

[34] K. Rubinur, P. Kharb, M. Das, P. T. Rahna, M. Honey, A. Paswan, S. Vaddi, and J. Murthy. A Multi-wavelength Study of the Dual Nuclei in Mrk 212. *Monthly Notices of the Royal Astronomical Society*, October 2020.

[35] Shobita Satyapal, Nathan J. Secrest, Claudio Ricci, Sara L. Ellison, Barry Rothberg, Laura Blecha, Anca Constantin, Mario Gliozzi, Paul McNulty, and Jason Ferguson. Buried AGNs in advanced mergers: Mid-infrared color selection as a dual AGN candidate finder. *The Astrophysical Journal*, 848(2):126, oct 2017.

[36] J. L. Sérscic. Influence of the atmospheric and instrumental dispersion on the brightness distribution in a galaxy. *Boletin de la Asociacion Argentina de Astronomia La Plata Argentina*, 6:41–43, February 1963.

[37] Jinyi Shangguan, Xin Liu, Luis C. Ho, Yue Shen, Chien Y. Peng, Jenny E. Greene, and Michael A. Strauss. Chandra x-ray and hubble space telescope imaging of optically selected kiloparsec-scale binary active galactic nuclei in ii. host galaxy morphology and agn activity. *The Astrophysical Journal*, 823(1):50, may 2016.

[38] Jack Sklansky. Finding the convex hull of a simple polygon. *Pattern Recognition Letters*, 1(2):79 – 83, 1982.

[39] Volker Springel, Simon D. M. White, Adrian Jenkins, Carlos S. Frenk, Naoki Yoshida, Liang Gao, Julio Navarro, Robert Thacker, Darren Croton, John Helly, John A. Peacock, Shaun Cole, Peter Thomas, Hugh Couchman, August Evrard, Jörg Colberg, and Frazer Pearce. Simulations of the formation, evolution and clustering of galaxies and quasars. *Nature*, 435(7042):629–636, Jun 2005.

[40] Stardate. *Double Trouble*, June 11, 2011 (accessed Nov 11, 2020). <https://stardate.org/astro-guide/gallery/double-trouble>.

[41] O. R. Vincent and O. Folorunso. Folorunso, "a descriptive algorithm for sobel image edge detection. In *in proceedings of Informing Science & IT Education Conference (InSITE*, 2009.

[42] Dawei Xu and S. Komossa. Narrow double-peaked emission lines of sdss j131642.90175332.5 : Signature of a single or a binary agn in a merger jet-cloud interaction, or unusual narrow-line region geometry. *The Astrophysical Journal*, 705(1):L20–L24, oct 2009.

[43] ZeeNews. *Nearby galaxy has two active black holes*, June 11, 2011 (accessed Nov 11, 2020). https://zeenews.india.com/news/space/nearby-galaxy-has-two-active-black-holes_712016.html.

[44] Hongyan Zhou, Tinggui Wang, Xueguang Zhang, Xiaobo Dong, and Cheng Li. Obscured Binary Quasar Cores in SDSS J104807.74+005543.5? *The Astrophysical Journal*, 604(1):L33–L36, March 2004.

A Details of GOTHIC

A.1 Scaling/Smoothening

FITS files deliver pixel intensity in units of nanomaggies. Due to shot noise, and possible numerical errors in the SDSS pipeline, some of the pixels have negative values for intensity. This is unphysical and such pixels need to be modified before the smoothening process. If this is not done, the log-normalisation produces a heavily skewed color-scaling, which is unfit for further processing. A $40''$ cutout centred around the object is taken. Then the maximum negative pixel value is found out in the cutout, which is subsequently added to all the pixels. To perform the log-normalisation, a lower and upper limit needs to be supplied, within which the normalisation would be conducted, subsequently followed by convolution with a 5×5 gaussian kernel -

$$\begin{aligned} lower &\leftarrow \max(0.1, \frac{\text{median}(\text{cutout})}{2}) \\ upper &\leftarrow \max(\text{cutout}) \end{aligned}$$

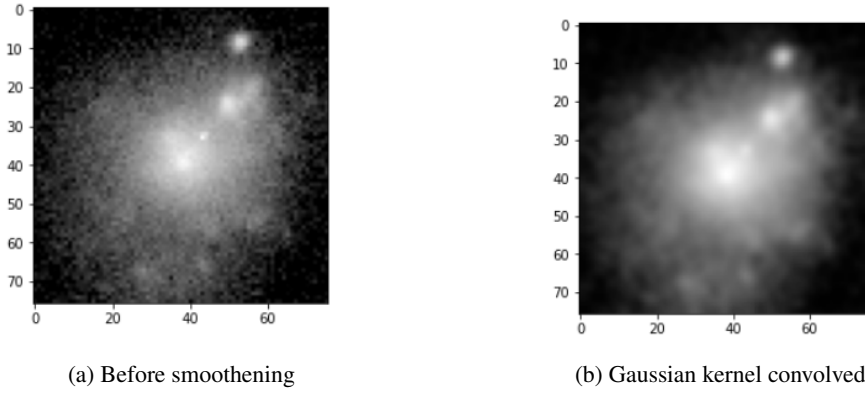


Figure 9: Smoothening Cutout Image

A.2 Edge Detection

Canny [10] has been used as the standard edge-detector. The edges detected do not necessarily correspond to the physical boundary of the object, since Canny utilizes the Sobel [41] operator which computes a first-order spatial derivative of the image. Using two kernels, the Sobel operator approximates $\frac{\partial}{\partial x}$ and $\frac{\partial}{\partial y}$ at every pixel which is subsequently replaced by $\sqrt{\left(\frac{\partial}{\partial x}\right)^2 + \left(\frac{\partial}{\partial y}\right)^2}$, that constitutes the magnitude of the edge.

Apart from the edges detected at the border of the galaxy envelope, it is possible that some edges of high magnitude are detected within it. Moreover, the edges at the envelope border don't necessarily form a closed figure. Hence, the convex hull [38] of the edges is used to bound the light envelope of the galaxy in a closed polygon. The statement of the convex hull problem is as follows - Given a set of points $S = \{(x_i, y_i)\}$, find the smallest convex subset H of S such that every member of S lies within the polygon defined by H . The definition of a convex subset H is as follows -

$$\begin{aligned} (x, y) &\in \text{interior}(H) \\ \forall (x, y) &\in L \\ \forall (x_1, y_1), (x_2, y_2) &\in \text{interior}(H) \end{aligned}$$

where L is the line-segment between (x_1, y_1) and (x_2, y_2) , and $\text{interior}(H)$ being the region contained by H . In other words, all points in any line segment within the interior of the hull, lie within the hull. Figure (A.10) shows this operation. The procedure accurately bounds the central galaxy within the cutout, however, it's possible it also includes stray foreground objects within the field of view. This is handled by the techniques discussed in (4.2)

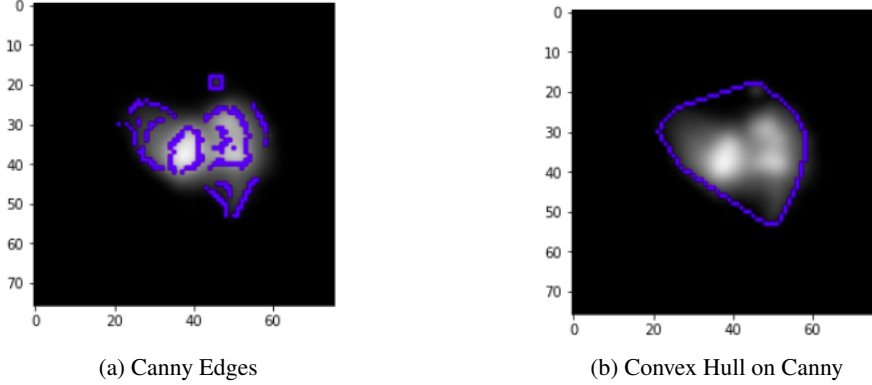


Figure 10: Edge Detection

A.3 Intensity Distribution Fitting

The convex hull method, as demonstrated above, usually encloses more than the galaxy envelope. Frequently, stray objects are enclosed within it. For bands with weak signals, the hull might enclose a large region without any appreciable signal. Thus, it is important to identify the pixel value which separates noise and signal. The Sersic [36] profile is widely used to fit the intensity distribution of galaxies. Intensity of light of a galaxy is taken to be a function of the radial distance from its centre. It is typically expressed in terms of the log of the intensity function. This form of is convenient as the original intensity data has been log-normalised. Hence, except by a constant factor, the sersic profile is applicable for intensity fitting -

$$\log I(R) = \log I_0 - kR^{\frac{1}{n}}$$

The parameter n is known as the sersic index, which characterises the shape of the plot. It has been stated in [11] that $1 \leq n \leq 15$ can fit most galaxies. However, we have found that $0.25 \leq n \leq 15$ gives a better fit for our purposes as we are observing the galaxies in 4 different bands.

A.3.1 Translating Frequency to Radius

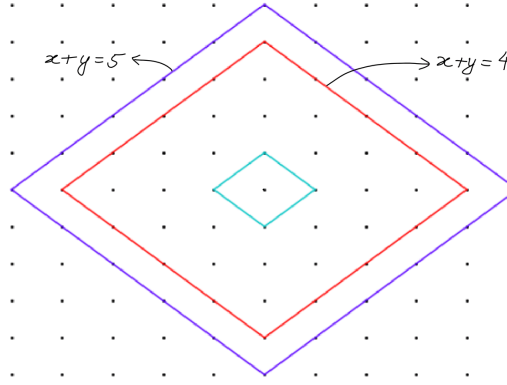


Figure 11: Solutions on Cartesian Grid

It is a simple matter to compute the histogram of the pixel intensity values. However, the sersic profile requires intensity values to be fit against radius from the centre of the galaxy, and not its respective frequency count. Thus, it's necessary to translate the frequency of pixel values to their distance from the centre of a galaxy. This is achieved by finding the number of solutions for (given R) -

$$\begin{aligned} x + y &= R \\ x, y &\in \mathbb{Z} \end{aligned}$$

Let the number of solutions be S_R . It can be seen that the enclosing rectangle for S_4 can be shifted one step outward, except the four vertices, to partially cover the edges of S_5 , after which 8 points would be remaining. Thus, the recurrence is -

$$S_{R+1} = (S_R - 4) + 8 = S_R + 4$$

The base case is $S_1 = 4$, which gives $S_R = 4R$. In another words, if the number of solutions is taken to be the frequency of a particular pixel value, then $f = 4R$

A.3.2 Setting the fit function

The maximum pixel value enclosed in the hull region, P_{max} , translates to $\log I_0$ as the cutout has been log-normalised. With $P(f)$ as the inverse of the pixel value-frequency histogram $f(P)$, the function to be fit for the parameters k, n is

$$P(f) = P_{max} - k \left(\frac{f}{4} \right)^{\frac{1}{n}}$$

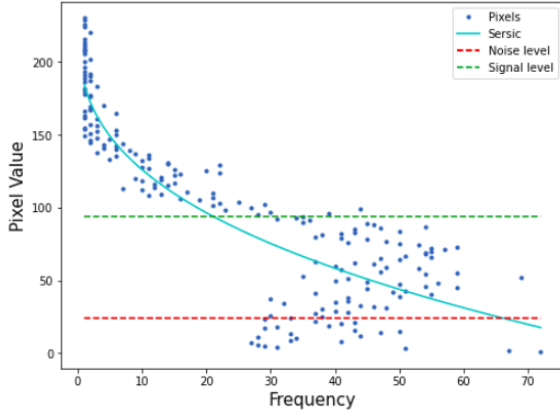


Figure 12: Fitting the Sersic Profile

A.3.3 Inferring the noise and signal levels

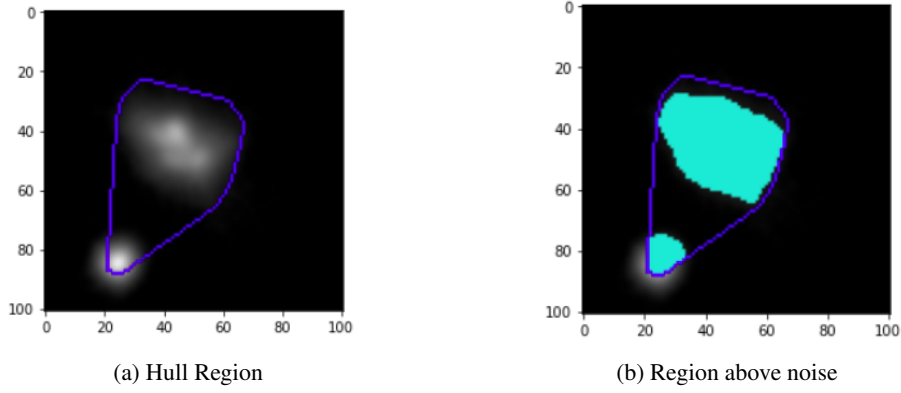


Figure 13

From the fit, the noise and signal levels are inferred which aid in searching the intensity peaks in the image. Peak searching is only performed in those regions that lie above the noise level (noise). This step is necessary as the residual coarseness of the image results in erroneous peaks. We infer the noise level from the radius at which the Sersic fit gives 95% of the integrated light. The signal level is also determined by the same process, but at 50% of the intergrated light, and referred to as (signal). The regions of the image above the noise level are marked in turquoise in figure (13b).